

Crustal structure across the Altyn Tagh Range at the northern margin of the Tibetan plateau and tectonic implications

Jungmeng Zhao ^{a,b}, Walter D. Mooney ^{c,*}, Xiankang Zhang ^d,
Zhichun Li ^e, Zhijun Jin ^f, Nihal Okaya ^c

^a *Institute of Tibetan Plateau Research, Chinese Academy of Sciences, Beijing, China*

^b *Institute of Geology, China Seismological Bureau, Beijing, China*

^c *U.S Geological Survey, 345 Middlefield Road, Menlo Park, CA 90425, USA*

^d *Geophysical Exploration Center, China Seismological Bureau, Zhengzhou, China*

^e *Institute of Occupational Disease Protection for Laboring Hygiene of Hunan Province, Changsha, China*

^f *Petroleum University, Beijing, China*

Received 14 June 2005; received in revised form 1 November 2005; accepted 1 November 2005

Available online 22 December 2005

Editor: S. King

Abstract

We present new seismic refraction/wide-angle-reflection data across the Altyn Tagh Range and its adjacent basins. We find that the crustal velocity structure, and by inference, the composition of the crust changes abruptly beneath the Cherchen fault, i.e., ~100 km north of the northern margin of the Tibetan plateau. North of the Cherchen fault, beneath the Tarim basin, a platform-type crust is evident. In contrast, south the Cherchen fault the crust is characterized by a missing high-velocity lower-crustal layer. Our seismic model indicates that the high topography (~3 km) of the Altyn Tagh Range is supported by a wedge-shaped region with a seismic velocity of 7.6–7.8 km/s that we interpret as a zone of crust–mantle mix. We infer that the Altyn Tagh Range formed by crustal-scale strike-slip motion along the North Altyn Tagh fault and northeast–southwest contraction over the range. The contraction is accommodated by (1) crustal thickening via upper-crustal thrusting and lower-crustal flow (i.e., creep), and (2) slip-parallel (SW-directed) underthrusting of only the lower crust and mantle of the eastern Tarim basin beneath the Altyn Tagh Range. © 2005 Elsevier B.V. All rights reserved.

Keywords: Altyn Tagh Range; Qaidam basin; Tarim basin; seismic and compositional structure of the crust and uppermost mantle; deformation processes; viscous sheet model; lower crustal flow/creep

1. Introduction

Northward convergence of India towards Asia since 55–65 Ma resulted in large-scale uplift of the Tibetan plateau to an average elevation of ~5 km [1,2]. At the

northern margin of the plateau, this convergence is absorbed by left-lateral strike-slip motion at the rate of 4–30 mm/y along the 1800-km-long Altyn Tagh fault [3–6] that created a steep topographic slope towards the Tarim basin to the north. Between 86°E and 92°E, however, the Altyn Tagh fault cuts through the plateau, with the high elevation Altyn Tagh Range rising to the north (Fig. 1).

There are two competing end-member models for the Cenozoic tectonics of the Tibetan plateau. In the

* Corresponding author. Tel.: +1 650 329 4764; fax: +1 650 329 5163.

E-mail addresses: zhaojm@itpcas.ac.cn (J. Zhao), mooney@usgs.gov (W.D. Mooney).

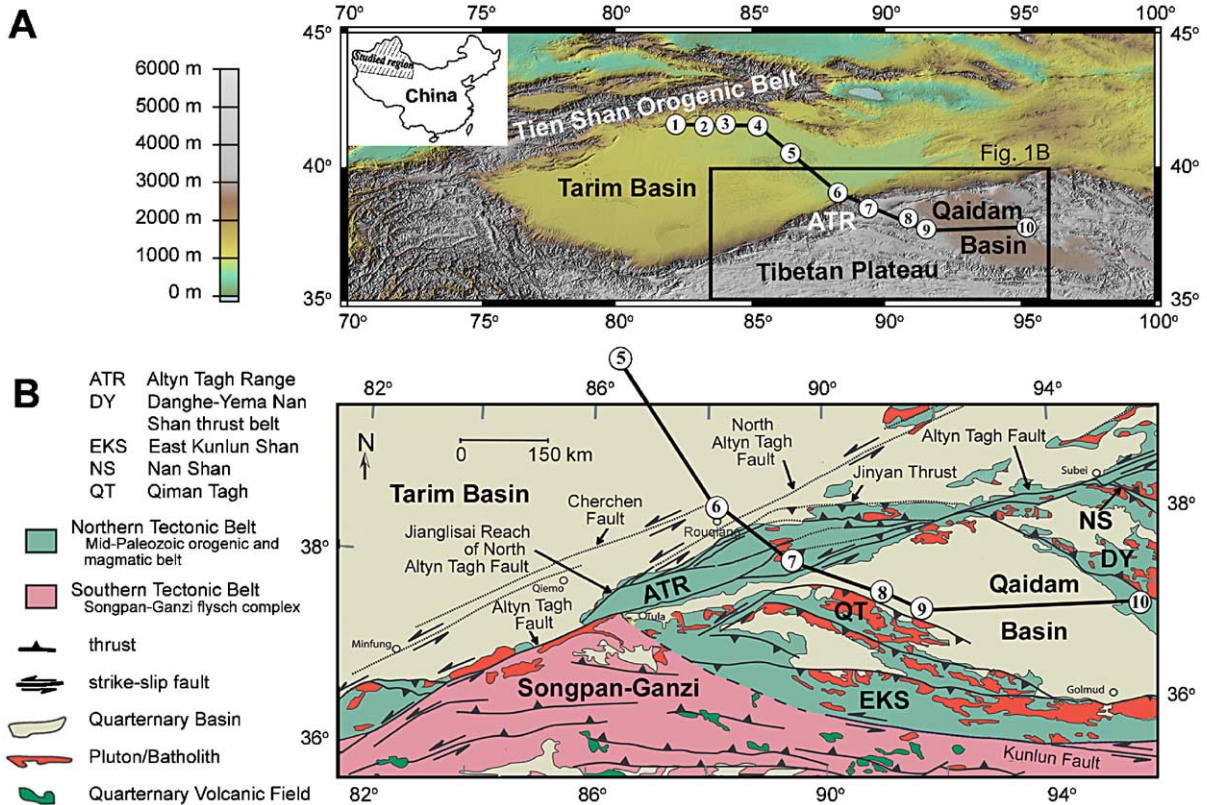


Fig. 1. (A) Topographic map of the Tarim basin and northern margin of Tibetan plateau. Shown is the location of the 1420-km-long seismic refraction/wide-angle-reflection profile extending from the northern margin of the Tarim basin to the eastern Qaidam basin. The circled numbers indicate shot points 1 to 10 of the seismic profile. The box indicates the area depicted in (B). (B) Tectonic map of the target area [26]; Shown is the section of the seismic profile and the shot points 5 to 10 (circled number) that we discuss in this paper.

rigid plate model, convergence is accommodated by discrete deformation along major thrusts and strike-slip faults bounding the blocks [7–10]. In the viscous sheet model, convergence is accommodated by crustal thickening via plastic creep within the soft middle/lower crust [11–17]. Diverse geologic and geophysical studies have investigated the northern margin of the Tibetan plateau [6,18–25]. While it is agreed that the Tarim basin is less deformed than the Tibetan Plateau, it is debated whether the rigid plate model or the viscous sheet model is more appropriate for the development of the Tarim–Tibet margin. Detailed knowledge of the crust and uppermost mantle across this margin can provide crucial constraints to resolve this controversy since the end-member models imply fundamentally different crustal structures.

Here we present the results of a 1420-km-long seismic refraction/wide-angle-reflection profile that crosses from NW to SE the northern margin of the Tarim basin, the east-central Tarim basin, the Altn Tagh Range, and the northern Qaidam basin (Fig. 1A). In our interpreta-

tion, we focus on the portion of the profile across the northern margin of the Tibetan plateau between shot point 5 and 10 (Fig. 1B).

2. The Altn Tagh Range

The 600-km-long rhomb-shaped Altn Tagh Range lies between the Tarim basin to the north and the Qaidam basin to the south (Fig. 1) and consists of Paleoproterozoic migmatite, gneiss, schist and Mesoproterozoic carbonates intruded by Proterozoic Paleozoic granitoids [27]. The Altn Tagh Range is bounded by the North Altn Tagh fault to the north, the Jinyan thrust to the northeast, and the Altn Tagh strike-slip fault to the south (Fig. 1B).

There are contrasting views about the tectonic deformational style of the Altn Tagh Range. In one interpretation, the main deformation is proposed to consist of southward wholesale underthrusting of the Tarim crust perpendicular to the North Altn Tagh fault and left-lateral strike slip along the Altn Tagh fault

[e.g., 20,28–31]. Alternatively, it has been proposed that the North Altyn Tagh fault and the Altyn Tagh fault form the northern and southern boundary of a strike-slip duplex within which transpressional deformation formed the Altyn Tagh Range [17,25]. The structure of the Altyn Tagh fault is also controversial. While some workers suggest that the Altyn Tagh fault is a crustal tear fault [2,28] other workers view the fault as a through-going lithospheric fault [20,10].

3. P-wave velocity and compositional structure

Seismic energy was generated by chemical explosions of 2 t TNT carried out at 10 shot points separated by 60–320 km (Fig. 1A). Ground motions were recorded on 204 portable 3-component seismographs spaced at an

interval of 1.5–3.0 km. Observed reduced record sections show very clear refracted and wide-angle reflected P-wave arrivals throughout the entire profile (e.g., shot point 6 to 9, Figs. 2A, 3A, 4A and 5A). Shot point 6 is located north of the Altyn Tagh fault and displays clear arrivals from within the crust and from the Moho (Fig. 2). All data are displayed without overlying traveltimes to avoid obscuring the arrivals. Shot point 7 is located within the Altyn Tagh Range and shows a very small delay time at the shot point due to the lack of sediments (Fig. 3). Further south, shot points 8 (Fig. 4) and 9 (Fig. 5) are located within the Qaidam basin and generate very clear data that include strong Moho reflections and refracted arrivals from the uppermost mantle (P_n). The data from all record sections yielded approximately 4000 P-wave picks from the arrivals (Fig. 6B).

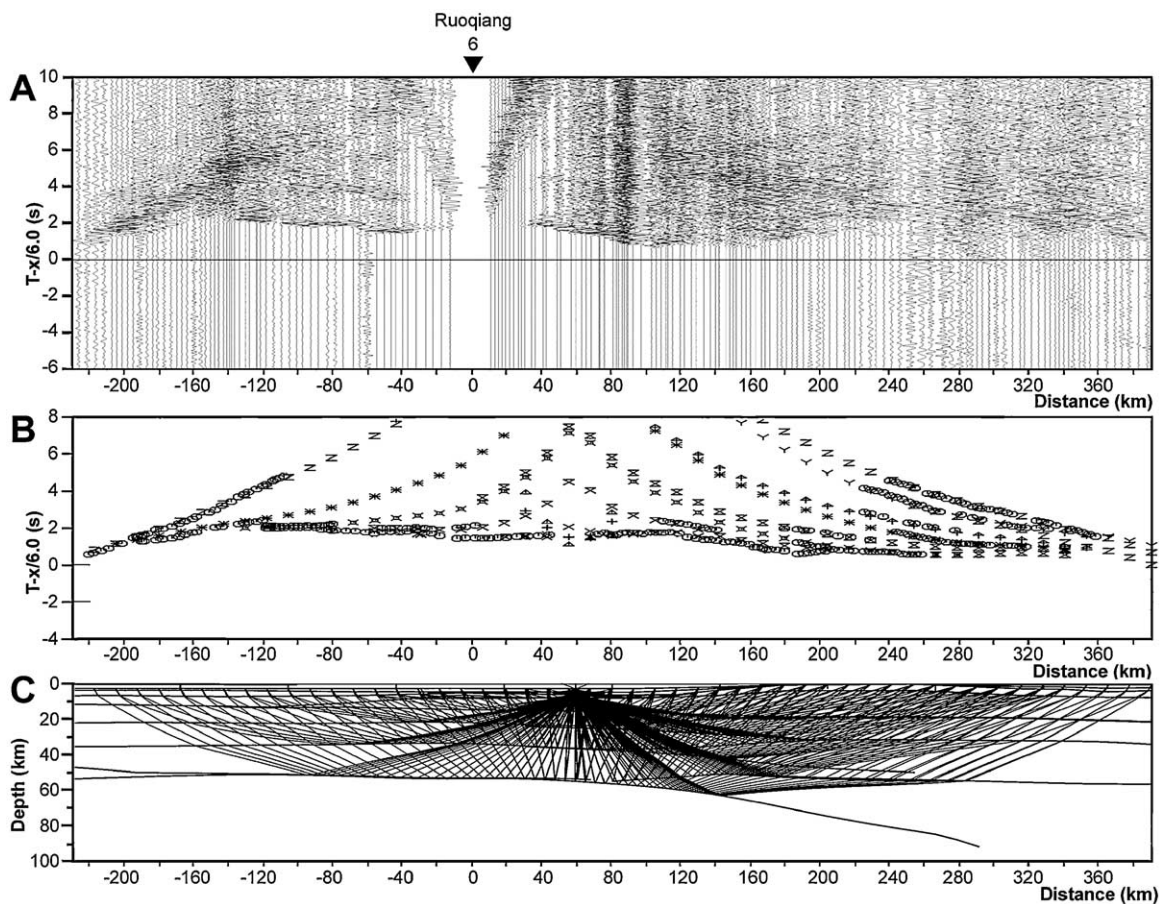


Fig. 2. Data and modeling example for shot point 6 (Ruoqiang): The shot point (at 0 km) is located north of the North Altyn Tagh fault in the Qaidam basin (c.f. Fig. 1B). The receivers were located in the Tarim basin, Altyn Tagh Range, and Qaidam basin. The horizontal axis indicates offset distance from the shot point. (A) Observed record section: The vertical axis indicates travel time reduced by 6 km/s. A 1–20 Hz bandpass filter and automatic gain control with 2-s window were applied. (B) Travel time fitting: The vertical axis indicates travel time measured (marked with \odot) and calculated (with other marks), reduced by 6 km/s. Travel times of all observed phases constitute the input data for ray tracing and synthetic seismogram. (C) Ray tracing: The vertical axis indicates depth in km. The thick lines are interfaces determined by modeling of the seismic phases. Vertical exaggeration 1:2.

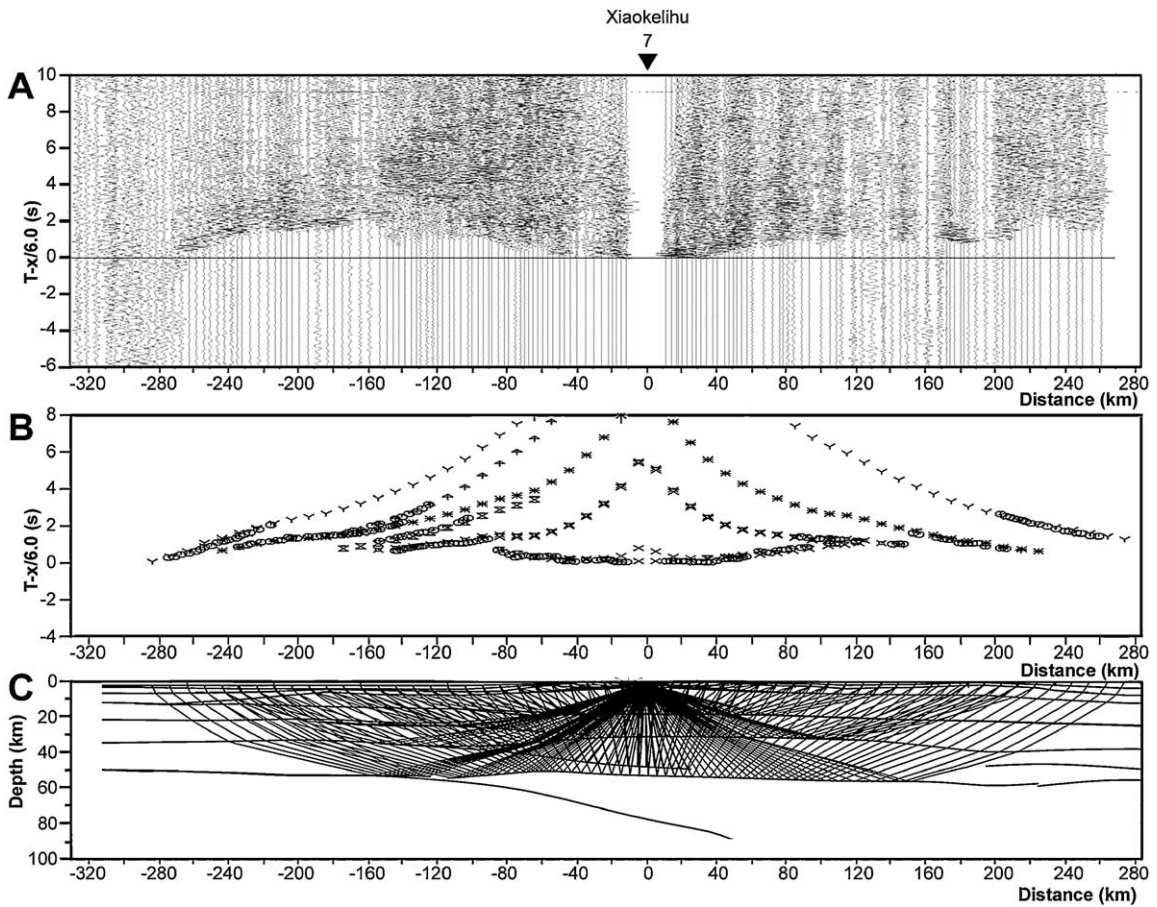


Fig. 3. Data and modeling example for shot point 7 (Xiaokeliu): The shot point (at 0 km) is located in the Altyn Tagh Range (c.f. Fig. 1B). The receivers were located in the Tarim basin, Altyn Tagh Range, and Qaidam basin. The horizontal axis indicates offset distance from the shot point. Presentation (panels A, B, C) as described in Fig. 2.

The two-dimensional compressional-wave velocity (V_p) structure of the crust and uppermost mantle along the profile was determined using the interactive program SEIS83 [32,33] which uses point-to-point ray tracing and calculates synthetic seismograms for two-dimensional Earth structures (Figs. 2–5, B and C). Ray tracing and synthetic seismograms were calculated for every shot point. The available traveltime and subsurface ray coverage are shown in Fig. 6A and B. Using this procedure we derived the two-dimensional velocity structure of the crust and uppermost mantle along the profile (Fig. 6C). The resulting V_p model is reliable in the area defined by dense ray coverage (Fig. 6B); outside this area the range is extrapolated. Trial-and-error tests indicate that the resulting V_p model has an uncertainty of 3% in regions of overlapping ray coverage.

We have used the seismic velocity structure (Fig. 6C) to estimate the composition of the crust and uppermost mantle (Fig. 7B) using laboratory measure-

ments of seismic velocities for a wide suite of rock types [34]. Within the crust, we identify six different layers ranging from sedimentary to mafic rocks. Below the crust we differentiate between a mixture of mafic crustal and ultramafic mantle rocks ($V_p=7.3\text{--}7.8$ km/s), and ultramafic mantle rocks ($V_p>7.8$ km/s). The near-surface layer has velocities of 4.6–5.7 km/s and is composed of sediments and crystalline basement rocks. The upper crust exhibits uniform velocities of 6.0–6.2 km/s indicative of a felsic composition. North of the Cherchen fault, ~100 km north of the North Altyn Tagh fault, seismic velocities in the middle ($V_p=6.6$ km/s) and lower Tarim crust ($V_p=6.9\text{--}7.25$ km/s) indicate an intermediate and mafic composition, respectively. South of the Cherchen fault, beneath the Altyn Tagh Range and Qaidam basin, velocities decrease to 6.3–6.4 km/s in the middle and 6.6–6.8 km/s in the lower crust implying a felsic and intermediate composition, respectively.

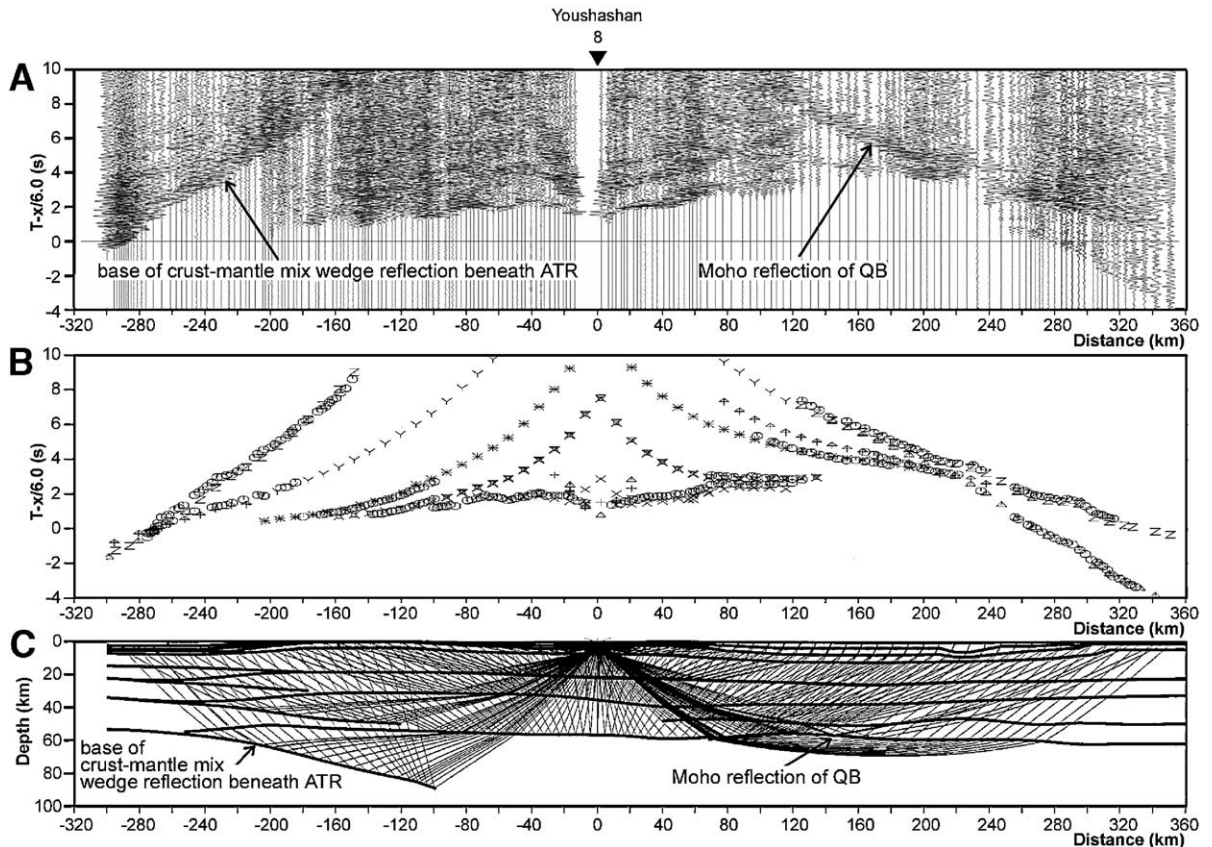


Fig. 4. Data and modeling example for shot point 8 (Youshashan): The shot point (at 0 km) is located south of the Altyn Tagh fault in the Qaidam basin (c.f. Fig. 1B). The receivers were located in the Tarim basin, Altyn Tagh Range, and Qaidam basin. The horizontal axis indicates offset distance from the shot point. Key: ATR, Altyn Tagh Range; QB, Qaidam basin. Presentation (panels A, B, C) as in Fig. 2.

Compared to various standard crustal types [34], the Tarim basin has a platform-like crust with a clear division into a felsic upper, intermediate middle, and mafic (high-velocity) lower crust. However, its 48-km-thick crust is thicker than the world-wide average of 43.5 km [34] due to a ~ 8 km overburden of sedimentary rocks. In contrast to the Tarim crust, the Tibetan crust lacks a high-velocity (≥ 6.8 km/s) mafic lower-crustal layer (Figs. 6C and 7B). Furthermore, the velocity-depth structures of the crystalline crust beneath the Altyn Tagh Range and Qaidam basin are very similar, suggesting that they are of the same provenance. This contradicts the interpretation that the Altyn Tagh Range is a flake of Tarim basement thrust towards the NNW [20,35]. Average upper-mantle V_p -velocities of 8.2 km/s beneath the Tarim and Qaidam basins are in agreement with previous seismic studies [36]. Inversion of shear wave and surface wave data [37] reveal high V_s -velocities in the upper Tarim mantle, and average to high V_s -velocities in the upper Qaidam mantle. Surface heat flow is 44 mW/m² in the Tarim basin and

56 mW/m² in the Qaidam basin, respectively [38]. These measurements indicate that beneath the Tarim basins the upper mantle is as cold as a continental shield. Beneath the Qaidam basin, seismic velocities as well as surface heat flow indicate average temperatures in the lower crust and upper mantle. Therefore, the difference in seismic velocities between the Tarim lower crust and the Qaidam lower crust can be attributed to a compositional change rather than a thermal perturbation.

One of the most prominent seismic arrivals is a strong wide-angle reflection (Fig. 4A) that defines a wedge-shaped low-velocity (7.6–7.8 km/s) region extending to ~ 90 km depth beneath the Altyn Tagh crust (Fig. 6C). We interpret these low velocities as a mixture of mafic crustal and ultramafic mantle material (Fig. 7B). This interpretation is also supported by isostatic considerations. The increase in elevation from ~ 1 km in the Tarim basin to ~ 3 km in the Altyn Tagh Range is accompanied by only a modest (5 km) increase in crustal thickness (Fig 7A and B) while crustal isostatic equilibrium requires a crustal thickening of

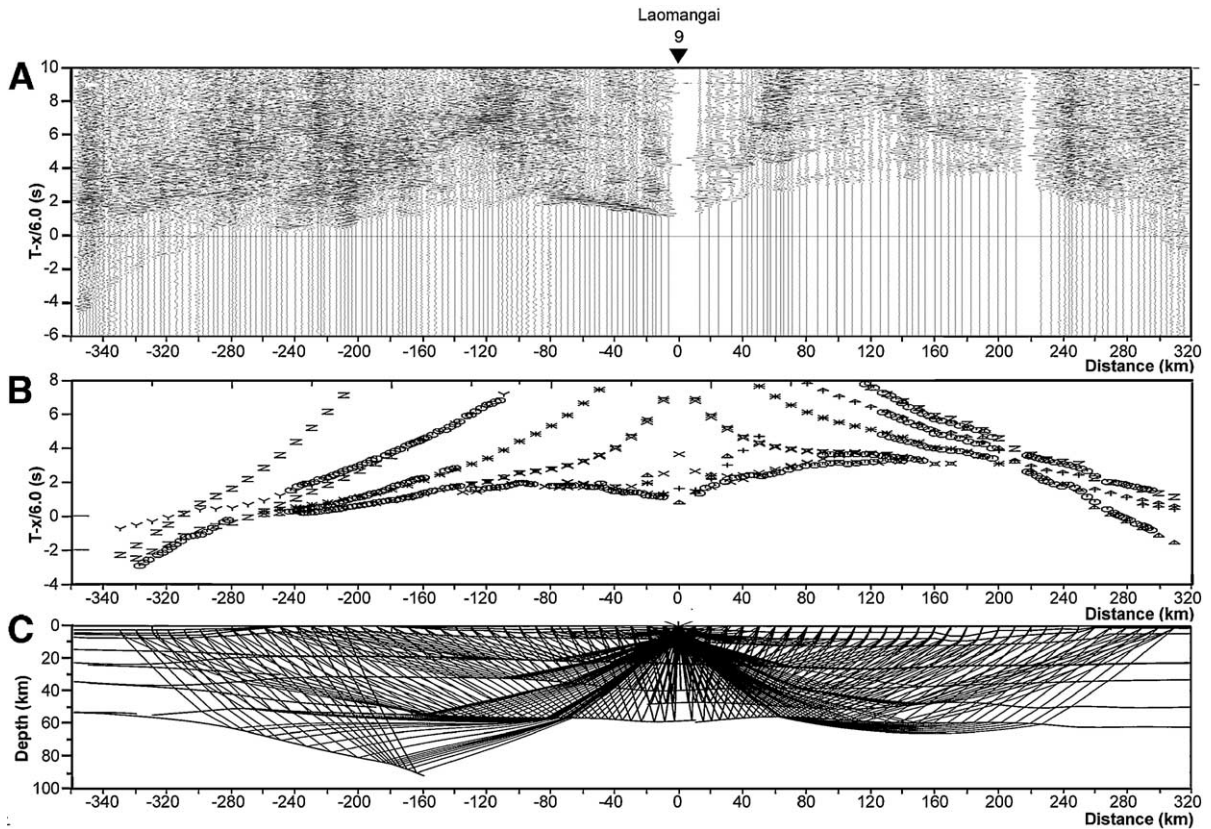


Fig. 5. Data and modeling example for shot point 9 (Laomangai): The shot point (at 0 km) is located south of the Altyn Tagh fault in the Qaidam basin (c.f. Fig. 1B). The receivers were located in the Tarim basin, Altyn Tagh Range, and Qaidam basin. The horizontal axis indicates offset distance from the shot point. Presentation (panels A, B, C) as in Fig. 2.

~14 km. We suggest that the elevation of the Altyn Tagh Range is supported by the low-density crust–mantle mix. A crust–mantle mix with a density deficit of 0.02 g/cm³ and an average thickness of 14 km could provide the necessary buoyancy. This is in good agreement with the 17.5 km average thickness of the wedge-shaped crust–mantle mix. Beneath the Altyn Tagh Range, our crustal model shows a thinned near-surface layer and oroclinal upper- and middle-crustal layers which indicate pronounced uplift and erosion. Present-day uplift rates of 3 ± 2 mm/y restricted to the Altyn Tagh Range [5] indicate that isostatic adjustment is still ongoing today.

4. Tectonic deformation processes

The contact between the Tarim basin and the Altyn Tagh Range has been hypothesized as a boundary with southeastward whole-crustal underthrusting of the Tarim basin, resulting in a crustal thickness of ~90 km beneath the Altyn Tagh Range [20]. Several features in our crustal velocity structure (Fig. 6C) are

irreconcilable with this model: (1) The minor 5-km-increase in crustal thickness between the Tarim basin (48 km) and the Altyn Tagh Range (53 km) excludes crustal doubling. (2) The sub-crustal low-velocity wedge beneath the Altyn Tagh Range represents a mixture of mafic lower crustal and ultra-mafic mantle material, which is inconsistent with whole-crustal underthrusting. (3) The distinct compositional change in the middle crust and lower crust ~100 km north of the Altyn Tagh Range (Fig. 7B) excludes underthrusting of the Tarim lower crust beneath the Altyn Tagh Range in a southeastward direction (i.e., along our seismic profile). If the mixture of mafic crustal and ultra-mafic mantle material beneath the Altyn Tagh crust were due to SE underthrusting of the Tarim lower crust we would expect to observe that the mafic lower crust beneath the Tarim basin (Fig. 7B) extends into the sub-crustal low-velocity wedge beneath the Altyn Tagh Range. Such a structure is not evident from our data.

We propose a new model (Fig. 8) where southwestward underthrusting of a sliver of the Tarim lower crust

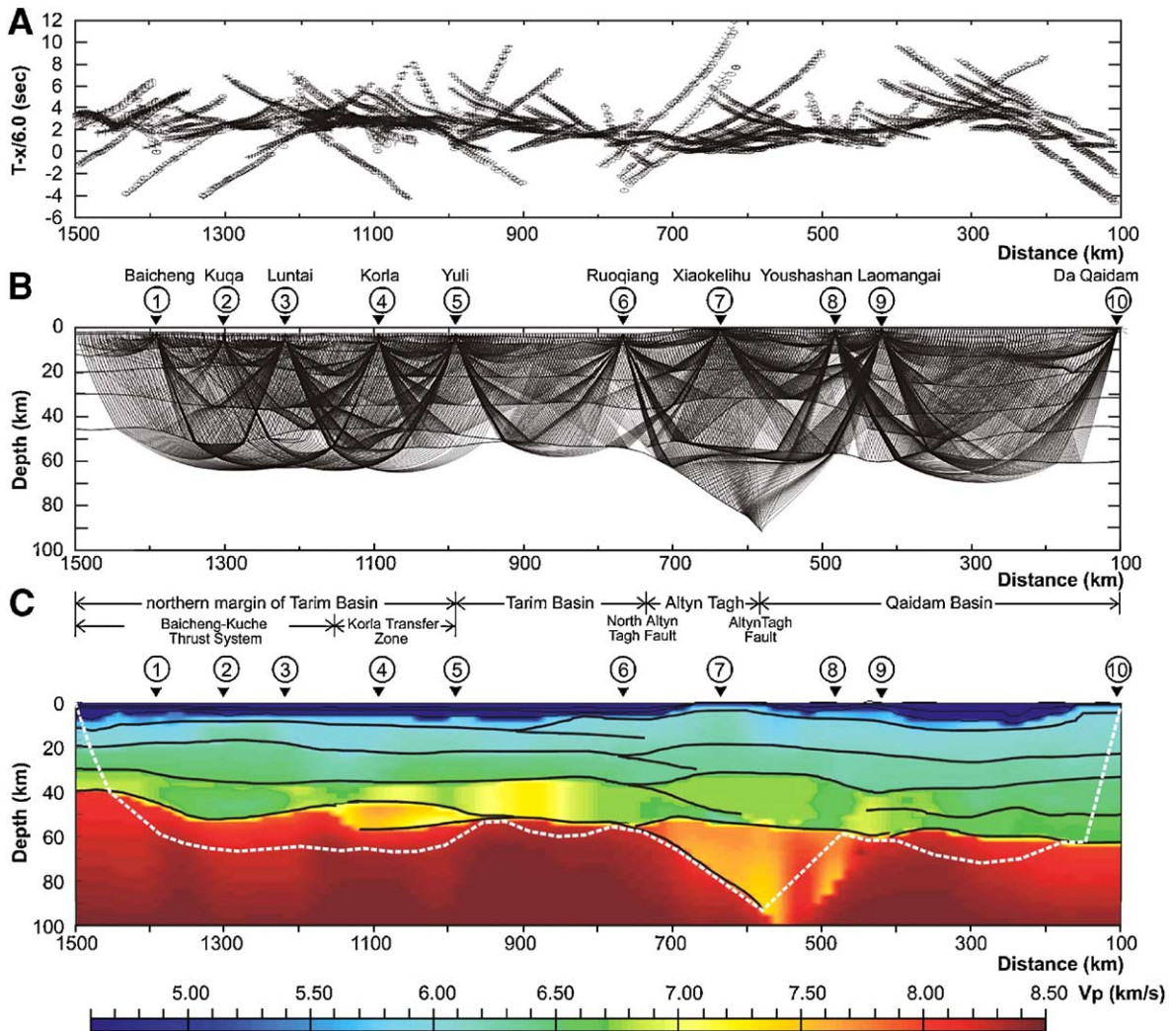


Fig. 6. Modeling results along the seismic refraction/wide-angle reflection profile from Baicheng (shot point 1) at the northern margin of the Tarim basin to Da Qaidam (shot point 10) at the eastern margin of the Qaidam basin. Circled numbers indicate shot point locations 1 to 10. The bent profile is projected onto a straight line; for profile and shot point locations see Fig. 1A. (A) Travel time fitting: Measured (marked with \odot) and calculated (with other marks) travel times for shot point 1 to 10. The vertical axis indicates travel time reduced by 6 km/s. Travel times of all observed phases constitute the input data for ray tracing and synthetic seismogram. (B) Ray tracing and effective ray coverage: The vertical axis indicates depth in km. The thick lines represent interfaces determined by wide-angle seismic reflection data. The program accomplishes point-to-point ray tracing and synthesis of seismograms for two-dimensional models. The results are shown with the vertical exaggeration 1:3. (C) Tectonic setting (upper panel), and final two-dimensional P-wave (V_p) velocity structure of the crust and uppermost mantle: The thick lines are interfaces determined by seismic wide-angle-reflection data. The region with dense ray coverage is indicated by a broken white line; outside this area velocities are inferred due to requirements of the modeling program. The results are shown with the vertical exaggeration 1:3.

and mantle underthrusts the Altyn Tagh Range oblique to the North Altyn Tagh fault. This process results in the wedge-shaped low-velocity zone beneath the Altyn Tagh crust seen in our V_p model (Fig. 6C). The North Altyn Tagh fault that separates the rigid Tarim basin from the soft Altyn Tagh Range accommodates primarily strike-slip motion and only minor fault-perpendicular thrusting, similar to an oblique thrust ramp, resulting in the steep topographic slope across the North Altyn

Tagh fault (Fig. 7A). Strike-slip faulting between the Tarim and Altyn Tagh crust explains the distinct compositional change in the middle and lower crust (Fig. 7B). Within the upper crust, southwest–northeast convergence is compensated by thrusting in the Jinyan thrust system resulting in the smooth topographic slope across the Jinyan thrust (Fig. 1). Within the lower crust, convergence is accommodated by plastic deformation and/or lower crustal creep. Our tectonic

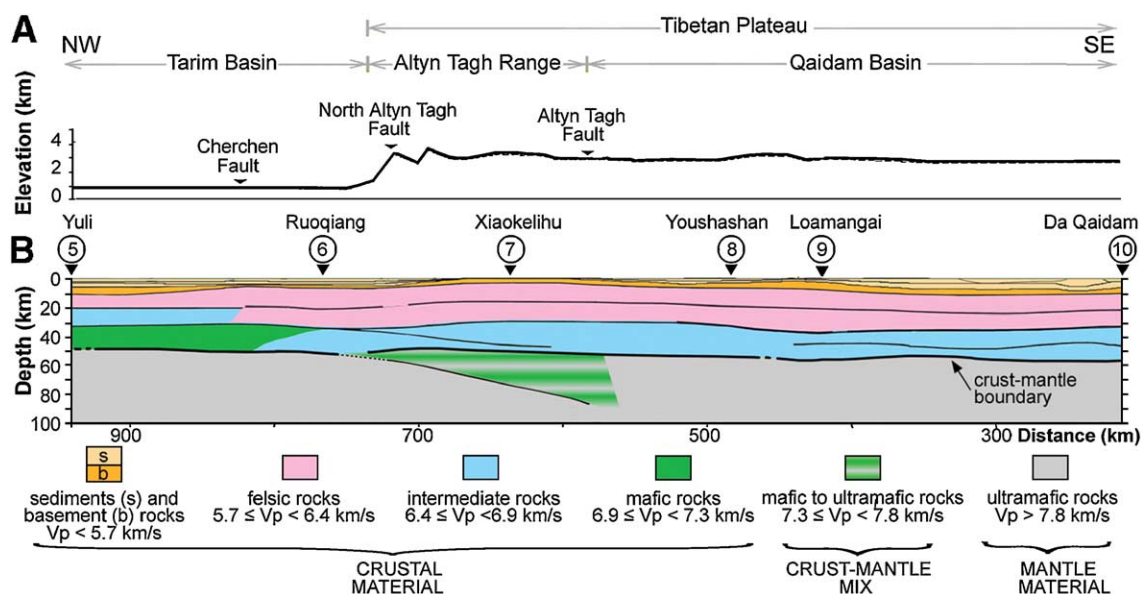


Fig. 7. Crustal and upper-mantle cross-section across the east-central Tarim basin, Altyn Tagh Range and Qaidam basin between shot point 5 and 10 (Fig. 1A): The bent profile is projected onto a straight line. (A) Tectonic setting (top panel) and topography (bottom panel): The major tectonic elements, faults and thrusts that our profile crosses are indicated. (c.f., Fig. 1B). The topography is shown with a vertical exaggeration of 1 : 10. (B) Two-dimensional compositional structure: The composition of the crust and uppermost mantle is derived from the seismic velocity structure (Fig. 6C) using laboratory measurements of seismic velocities for a wide suite of rock types [1]. Within the crust, we identify six layers ranging from sedimentary to mafic rocks. Below the crust we distinguish between a mixture of mafic crustal and ultramafic mantle rocks (7.3–7.8 km/s), and ultramafic mantle rocks (>7.8 km/s). The results are shown with the vertical exaggeration 1 : 3.

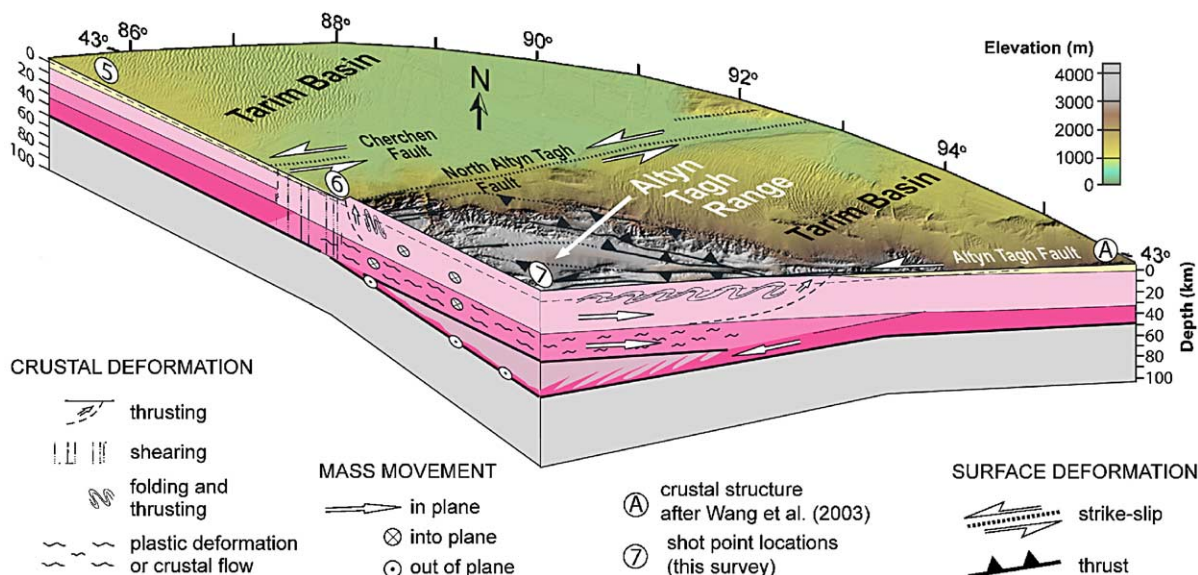


Fig. 8. Schematic three-dimensional crustal section across the Tarim basin and Altyn Tagh Range illustrating the proposed deformation processes active at the northern margin of the Tibetan plateau: Yellow corresponds to Cenozoic sediments and basement rocks. Pink shows crustal rocks with lighter and darker colors indicating low and high P-wave velocities, respectively. Circled numbers indicate shot point locations of our seismic survey. The crustal structure beneath the circled number A is after Wang et al. [42]. Convergence is accommodated: (1) in the upper crust by strike-slip along the North Altyn Tagh fault and slip-parallel thrusting, (2) in the lower crust by slip-parallel (northeastward) flow (i.e., creep), and (3) in the upper mantle by slip-parallel (southwestward) underthrusting of only the Tarim lower crust and mantle beneath the Altyn Tagh Range.

deformation model is supported by diverse geologic and geophysical observations which we discuss in the following.

Strike-slip motion along the North Altyn Tagh fault is supported by several other observations. Fault offset features document left-lateral slip of ~ 120 km at the Jianglisai reach of the North Altyn Tagh fault [25] (Fig. 1B). Southwest underthrusting of the Tarim lower crust and mantle perpendicular to the Jinyang thrust would amount to ~ 160 km which is in the same order of magnitude as left-lateral slip along the Jianglisai reach of the North Altyn Tagh fault. Shear wave splitting with a fast polarization direction oriented $\sim N60^\circ E$ beneath the Altyn Tagh Range implies creep of the crust and mantle parallel to the North Altyn Tagh fault [23].

Our high-resolution image of the crust shows that the crust–mantle boundary beneath the Altyn Tagh Range and Qaidam basin is flat (Fig. 6C). Deformation accommodated by lower crustal creep can explain a uniformly elevated mountain range that is underlain by a flat crust–mantle boundary [39]. A soft and viscous lower crust capable of creep is supported by our crustal model that shows an intermediate composition of the lower Altyn Tagh and Qaidam crust at depths where temperatures typically reach $\sim 500^\circ C$ (Fig. 7B). Our observations, therefore, support not just plastic deformation but channel flow (i.e., creep in the lower Altyn Tagh and Qaidam crust (Fig. 8). Lower-crustal flow has been proposed as the dominant mechanism for the formation of the eastern Tibetan Plateau [15,16].

Previous studies of the India–Asia collision zone have reported offsets at the crust–mantle boundary beneath major strike-slip faults. Such offsets are thought to be characteristic of those strike-slip faults that pass through the lithosphere [40–42]. Based on tomographic imaging it has been suggested that the Altyn Tagh fault is a lithospheric-scale boundary where crustal deformation within the Altyn Tagh Range is backstopped, resulting in a major step at the Moho [20]. In contrast, our V_p model shows a flat and uninterrupted crust–mantle boundary between the Altyn Tagh Range and Qaidam basin (Fig. 6C). This may indicate that the Altyn Tagh fault is confined to the crust, as has been previously suggested [18,43]. Seismic profiles and receiver functions located south of our study area (i.e., on the Tibetan plateau south of the Qaidam basin) show a crust that: (1) contains a prominent mid-crustal low velocity zone, which we do not identify, and (2) is 10–25 km thicker than reported here [44,45].

Recent GPS results have suggested that the slip rate along the Altyn Tagh fault is roughly 9 mm/yr [46,47], significantly lower than geological estimates of 20–30

mm/yr [48]. The total shear strain rates required to accommodate the approximately 25 mm/yr of eastward motion of eastern Tibet with respect to the Tarim Basin, as indicated by GPS estimates [47], significantly exceeds the geodetically observed slip rate, and hence shear strain rates, on the Altyn Tagh fault. This suggests that slip is accommodated on one or more faults in north-central Tibet, with the Kunlun fault, which recently experienced a $M_w=7.8$ earthquake, being a prime candidate.

5. Summary

We report results from an active-source seismic refraction profile across the Altyn Tagh Range at the northern margin of the Tibetan Plateau. Below a thick (8 km) blanket of sediments, the eastern Tarim basin has a crustal structure that is typical of stable continental platforms, with a clear division into a felsic upper, intermediate middle and mafic (high-velocity) lower crust. In contrast, the crust beneath the northern Tibetan plateau lacks a high-velocity mafic lower crustal layer. The velocity–depth structures of the Altyn Tagh Range and the Qaidam basin are very similar, suggesting that they are of the same provenance.

The crust of the Altyn Tagh Range is underlain by a wedge-shaped low-velocity region that extends to a depth of ~ 90 km. We interpret this low-velocity wedge to consist of a mixture of mafic crustal and ultramafic mantle material. The buoyancy of the low-density wedge is sufficient to provide the elevation of the Altyn Tagh Range.

We propose a new tectonic model for the Altyn Tagh Range that incorporates southwestward underthrusting of a sliver of the easternmost Tarim lower crust and upper mantle at an oblique angle to the Altyn Tagh fault and northeast–southwest contraction within the Altyn Tagh Range. This geometry results in thrust faulting, uplift, and the observed wedge-shaped region of crust–mantle mix.

The Moho boundary beneath the Altyn Tagh Range and Qaidam basin is flat, which suggests that this region of active deformation is accommodated by lower crustal plastic deformation and/or lateral flow (i.e., creep). Furthermore, our data indicate that the Moho is not offset beneath the Altyn Tagh fault, as has been suggested from receiver function analysis for the southern boundary of the Qaidam basin [40]. Our crustal model, combined with other observations, suggests that the North Altyn Tagh fault separates the rigid platform-type crust of the Tarim basin from the soft, deforming crust of the Tibetan plateau.

Acknowledgements

We thank E. Cowgill, A. Kelly, J. Murray, J. Ritsema, W. Thatcher, S. King and two anonymous reviewers for comments that have greatly helped to improve the manuscript. We also thank S.B. Bozkurt for creating the topographic image.

References

- [1] P. Molnar, A review of geophysical constraints on the deep structure of the Tibetan Plateau, the Himalaya and the Karakoram, and their tectonic implications, *Philos. Trans. R. Soc. Lond. Ser. A* 326 (1988) 33–88.
- [2] A. Yin, T.M. Harrison, Geologic evolution of the Himalayan–Tibetan Orogen, *Annu. Rev. Earth Planet. Sci.* (2000) 211–280.
- [3] G. Peltzer, P. Tapponnier, R. Amijio, Magnitude of Late Quaternary left-lateral displacements along the north edge of Tibet, *Science* 246 (1989) 1285–1289.
- [4] B. Meyer, P. Tapponnier, Y. Gaudemer, G. Peltzer, S. Guo, Z. Chen, Rates of left lateral movement along the easternmost segment of the Altyn Tagh fault, east of 96°E (China), *Geophys. J. Int.* 124 (1996) 29–44.
- [5] R. Bendick, R. Bilham, J. Freymueller, K. Larson, G. Yin, Geodetic evidence for low slip rate in the Altyn Tagh fault system, *Nature* 424 (2000) 69–72.
- [6] Z. Shen, M. Wang, Y. Li, D.D. Jackson, A. Yin, D. Dong, P. Fang, Crustal deformation along the Altyn Tagh fault system, western China, from GPS, *J. Geophys. Res.* 106 (2001) 30607–30621.
- [7] P. Tapponnier, P. Molnar, Slip-line field theory and large-scale continental tectonics, *Nature* 264 (1976) 319–324.
- [8] G. Peltzer, P. Tapponnier, Formation and evolution of strike-slip faults, rifts, and basins during the India–Asia collision: an experimental approach, *J. Geophys. Res.* 93 (1988) 15085–15117.
- [9] X. Kong, P. Bird, Neotectonics of Asia: thin-shell finite-element models with faults, in: A. Yin, T.M. Harrison (Eds.), *The Tectonic Evolution of Asia*, Cambridge Univ. Press, New York, 1996, pp. 18–34.
- [10] P. Tapponnier, Z. Xu, F. Roger, B. Meyer, N. Arnaud, G. Wittlinger, J. Yang, Oblique stepwise rise and growth of the Tibet Plateau, *Science* 294 (2001) 1671–1677.
- [11] P. England, D.P. McKenzie, A thin viscous sheet model for continental deformation, *Geophys. J. R. Astron. Soc.* 70 (1982) 295–321.
- [12] J.P. Vilotte, M. Daignie`res, R. Madariaga, Numerical modeling of intraplate deformation: simple mechanical models of continental collision, *J. Geophys. Res.* 87 (1982) 10709–10728.
- [13] P. England, G. Houseman, The mechanics of the Tibetan Plateau, *Philos. Trans. R. Soc. Lond. Ser. A* 326 (1988) 301–320.
- [14] P. Bird, Lateral extrusion of lower crust from under high topography in the isostatic limit, *J. Geophys. Res.* 96 (1991) 10275–10286.
- [15] L.H. Royden, B.C. Burchfiel, R.W. King, E. Wang, Z. Chen, F. Shen, Y. Liu, Surface deformation and lower crustal flow in eastern Tibet, *Science* 276 (1997) 788–790.
- [16] M.K. Clark, L.H. Royden, Topographic ooze: building the eastern margin of Tibet by lower crustal flow, *Geology* 28 (2000) 703–706.
- [17] F. Shen, L.H. Royden, B.C. Burchfiel, Large-scale crustal deformation of the Tibetan Plateau, *J. Geophys. Res.* 106 (2001) 6793–6816.
- [18] S.D. Willett, C. Beaumont, Subduction of Asian lithospheric mantle beneath Tibet inferred from models of continental collision, *Nature* 369 (1994) 642–645.
- [19] D.A. Griot, J.P. Montagner, P. Tapponnier, Phase velocity structure from Rayleigh and Love waves in Tibet and its neighboring regions, *J. Geophys. Res.* 103 (1998) 21215–21232.
- [20] G. Wittlinger, P. Tapponnier, G. Poupinet, J. Mei, S. Danian, G. Herquel, F. Masson, Tomographic evidence for localized lithospheric shear along the Altyn Tagh fault, *Science* 282 (1998) 74–76.
- [21] X. Jiang, N. Jin, M.K. McNutt, Lithospheric deformation beneath the Altyn Tagh and West Kunlun faults from recent gravity surveys, *J. Geophys. Res.* 109 (2004) B05426, doi:10.1029/2003/JB002444.
- [22] H. Kao, R. Gao, R.J. Rau, D. Shi, R.Y. Chen, Y. Guan, F.T. Wu, Seismic image of the Tarim basin and its collision with Tibet, *Geology* 29 (2001) 575–578.
- [23] G. Herquel, P. Tapponnier, G. Wittlinger, J. Mei, S. Danian, Teleseismic shear wave splitting and lithospheric anisotropy beneath and across the Altyn Tagh fault, *Geophys. Res. Lett.* 26 (21) (1999) 3225–3228.
- [24] A. Yin, P.E. Rummelhart, R. Buttler, E. Cowgill, T.M. Harrison, D.A. Forster, R.V. Ingersoll, Z. Qing, Z. Xian-Qiang, W. Wiaofeng, A. Hanson, A. Raza, Tectonic history of the Altyn Tagh fault system in northern Tibet inferred from Cenozoic sedimentation, *GSA Bull.* 114 (10) (2002) 1257–1295.
- [25] E. Cowgill, A. Yin, W.X. Feng, Z. Qing, Is the North Altyn fault part of a strike-slip duplex along the Altyn Tagh fault System?, *Geology* 28 (2000) 255–258.
- [26] E. Cowgill, A. Yin, T.M. Harrison, Reconstruction of the Altyn-Tagh fault based on U–Pb geochronology: role of back thrusts, mantle sutures, and heterogeneous crustal strength in forming the Tibetan Plateau, *J. Geophys. Res.* 108 (B7) (2003), doi:10.1029/2002JB002080.
- [27] XBGMR 1993 (Xinjiang Bureau of Geology and Mineral Resources) Regional geology of Xinjiang Uygur autonomous region: geological memoirs, Ser. 1, no. 32, Beijing, Geological Publishing House, 843 pp., scale 1:1,500,000.
- [28] P. Molnar, B.C. Burchfiel, Z.Y. Zhao, K.Y. Liang, S.J. Wang, M.M. Huang, Geological evolution of northern Tibet: results of an expedition to Ulugh Muztagh, *Science* 235 (1987) 299–305.
- [29] B.C. Burchfiel, D. Quidong, P. Molnar, L. Royden, W. Yipeng, Z. Peizhen, Z. Weiqi, Intracrustal detachment zones of continental deformation, *Geology* 17 (1989) 448–452.
- [30] J.P. Avouac, P. Tapponnier, Kinematic model of active deformation in central Asia, *Geophys. Res. Lett.* 20 (1993) 895–898.
- [31] G. Peltzer, F. Saucier, Present-day kinematics of Asia derived from geologic fault rates, *J. Geophys. Res.* 101 (27) (1996) 943–27956.
- [32] V. Cervený, I.A. Molotkov, I. Psencik, *Ray Method in Seismology*, Charles University Press, Prague, 1977, 214 pp.
- [33] V. Cervený, I.A. Molotkov, I. Psencik, *Ray Method in Seismology*, Charles University Press, Prague, 1977, pp. 57–120.
- [34] N.I. Christensen, W.D. Mooney, Seismic velocity structure and composition of the continental crust: a global view, *J. Geophys. Res.* 100 (1995) 9761–9788.
- [35] B. Meyer, P. Tapponnier, L. Bourjot, F. Metivier, Y. Gaudemer, et al., Crustal thickening in Gansu–Qinghai, lithospheric mantle

- subduction, and oblique, strike-slip controlled growth of the Tibet plateau, *Geophys. J. Int.* 135 (1998) 1–47.
- [36] C. Liang, X. Song, J. Huang, Tomographic inversion of Pn travel-times in China, *J. Geophys. Res.* 109 (2004), doi:10.1029/2003JB002789.
- [37] W. Friedrich, The S-velocity structure of the East Asian mantle from inversion of shear and surface waveforms, *Geophys. J. Int.* 153 (2003) 88–102.
- [38] Y. Wang, Heat flow pattern and lateral variations of lithospheric strength in China mainland: constraints on active deformation, *Phys. Earth Planet. Inter.* 126 (2001) 121–146.
- [39] L.H. Royden, Coupling and decoupling of crust and mantle in convergent orogens: implications for strain partitioning in the crust, *J. Geophys. Res.* 101 (B8) (1996) 17679–17705.
- [40] L. Zhu, D.W. Helmberger, Moho offset across the northern margin of the Tibetan plateau, *Science* 281 (1998) 1170–1172.
- [41] J. Vergne, G. Wittlinger, Q. Hui, P. Tapponnier, G. Poupinet, J. Mei, G. Herquel, A. Paul, Seismic evidence for stepwise thickening of the crust across the NE Tibetan plateau, *Earth Planet. Sci. Lett.* 203 (2002) 25–53.
- [42] G. Wittlinger, J. Vergne, P. Tapponnier, V. Farra, G. Poupinet, M. Jiang, H. Su, G. Herquel, A. Paul, Teleseismic imaging of subducting lithosphere and Moho offset beneath western Tibet, *Earth Planet. Sci. Lett.* 221 (2004) 117–130.
- [43] Y. Wang, W.D. Mooney, X. Yuan, R.G. Coleman, The crustal structure from the Altai Mountains to the Altyn Tagh fault, northwest China, *J. Geophys. Res.* 108 (B6) (2003), doi:10.1029/2001JB000552.
- [44] K.D. Nelson, W.J. Zhao, et al., Partially molten middle crust beneath southern Tibet: synthesis of Project INDEPTH results, *Science* 274 (1996) 1684–1688.
- [45] R. Kind, X. Yuan, J. Saul, D. Nelson, S.V. Sobolev, J. Mechie, W. Zhao, G. Kosarev, J. Ni, U. Auchauer, M. Jiang, Seismic images of crust and upper mantle beneath Tibet: evidence for Eurasian plate subduction, *Science* 298 (2002) 1219–1221.
- [46] R. Bendick, R. Bilham, J.T. Freymueller, K.M. Larson, G.H. Yin, Geologic evidence for a low slip rate in the Altyn Tagh fault system, *Nature* 404 (2000) 69–72.
- [47] Z.K. Shen, M. Wang, Y. Li, D.D. Jackson, A. Yin, D. Dong, P. Fang, Crustal deformation along the Altyn Tagh Fault system, western China, from GPS, *J. Geophys. Res.* 106 (2001) 30,607–30,621.
- [48] G. Peltzer, P. Tapponnier, R. Armijo, Magnitude of the Late Quaternary left-lateral displacements along the north edge of Tibet, *Science* 246 (1989) 1285–1289.